Journal of Power Sources 250 (2014) 220–235

Contents lists available at ScienceDirect

Journal of Power Sources

journal homepage: www.elsevier.com/locate/jpowsour

Mathematical model for a spirally-wound lithium-ion cell

Meng Guo, Ralph E. White*

Department of Chemical Engineering, University of South Carolina, 301 Main Street, Columbia, SC 29208, USA

HIGHLIGHTS

- A mathematical model for the thermal behavior of a wound cylindrical Li-ion cell was developed.
- The new numerical method significantly saves computation time and memory allocation.
- The coordinate transform and variable extrusion algorithms were validated.

ARTICLE INFO

Article history:
Received 24 September 2013
Received in revised form
7 November 2013
Accepted 11 November 2013
Available online 19 November 2013

Keywords:
Li-ion cell
Jelly-roll
Spiral wound
Charge balance
Thermal model

ABSTRACT

A new computational method is proposed that can be used to reduce the numerical difficulties in modeling the electrical and thermal behavior of a spirally wound Li-ion cell. By analyzing the winding locus of the electrodes, some important geometric relationships of the spiral surfaces are identified, and algorithms for coordinate transform and variable extrusion between 2-D and 3-D domains are derived. Our method reduces the computation time and memory requirements needed to simulate the cell performance. The accuracy of our method was validated by model-to-model comparisons.

1. Introduction

Today, most of the safety issues for Li-ion cells and batteries are related to the electrical and thermal properties of the composite electrodes. [1–4] Therefore, mathematical models that deal with the charge balance and heat transfer in cells have become important tools for cell design. However, the implementation of these models is significantly affected by the cell geometry and electrode configurations. There are basically two types of electrode structures in Li-ion cells, the laminated or pouch structure and the wound structure. For the laminated electrode structure, all the electrodes are flat and arrayed in parallel, and the transfer of charge and energy goes along the orthogonal directions in the Cartesian coordinate system. Therefore, building and meshing the computational domains for laminated electrodes can be done easily in commercial CAD software. For the wound electrode structure, however, the electrodes are put through a complicated winding locus, and the electrical potentials of the solid phases are non-continuous along the normal direction of the winding surface due to the insulating separator layer. Therefore, electrical insulation zones with full winding details must be included in the model domains for wound electrodes, and the meshing of these domains becomes extremely difficult if the electrodes have many winding turns.

Due to the numerical difficulties discussed above, most 3-D physical models have been developed for cells with laminated electrodes [5–9], and modeling for the wound-structure electrodes have been rarely reported. Gomadam et al. [10] developed a 2-D thermal model for a cylindrical jell-roll based on the spiral geometry relations, but the charge balances in the current collector foils, which are supposed to be the most difficult parts for the wound electrode models, were neglected. Santhanagopalan et al. [11] and Ye et al. [12] also developed physics-based models for the wound cells, but their models are limited to 2-D. In a recent paper by Lee et al. [13], a multi-scale multi-dimensional (MSMD) model for wound cells was reported; however, their approach involves two mesh groups in which the size for geometry units are no larger than twice the electrode pair

* Corresponding author. Tel.: +1 803 777 3270.
E-mail address: white@cec.sc.edu (R.E. White).

0378-7753/$ – see front matter © 2013 Published by Elsevier B.V.
http://dx.doi.org/10.1016/j.jpowsour.2013.11.023

thickness, and thus requires a large number of mesh elements which would make the model computationally expensive.

In this work, a new modeling approach different from all the above-mentioned ones is developed. The charge balance and heat transfer in a jelly-roll are solved separately in different computational domains, and coupled through a coordinate transform and variable extrusion algorithm derived from analytical geometry relationships. The mesh requirement for the 3-D domain is significantly lowered by using these geometric algorithms.

2. Mathematical approach

2.1. Basic geometric relations

Our model was developed from an assumption that all the cell sandwich layers (current collectors, coatings, and the separator) in the jelly-roll of a18650-type cylindrical cell are of uniform thicknesses and are wound through an Archimedean spiral locus which can be described by the following polar coordinate equation:

$$r = r_0 + \frac{D}{2\pi}\theta \tag{1}$$

where r is the radius coordinate, θ is the angular coordinate, r_0 is the initial radius of the spiral at $\theta = 0$, and D is the separation distance. The geometry details for a spiral surface are presented in Fig. 1, where the surface is wound spirally around the z axis and the cross section on the x–y plane is an Archimedean spiral curve described by Equation (1). The Archimedean spiral has the property that any ray from the origin intersects successive turnings of the spiral in points with a constant separation distance D, and the difference in the polar angle between two intersecting points, $\Delta\theta$, is 2π. In Fig. 1, ξ is the tangential arc length along the spiral curve and differentiation of ξ can be expressed as follow:

$$\mathrm{d}\xi = \sqrt{r^2 + \left(\frac{\mathrm{d}r}{\mathrm{d}\theta}\right)^2}\,\mathrm{d}\theta = \sqrt{\left(r_0 + \frac{D}{2\pi}\theta\right)^2 + \left(\frac{D}{2\pi}\right)^2}\,\mathrm{d}\theta \tag{2}$$

A functional relationship between the arc length ξ and the polar angle θ can be derived by integrating Equation (2):

$$\begin{aligned}\xi(\theta) &= \int_0^\theta \sqrt{r^2 + \left(\frac{\mathrm{d}r}{\mathrm{d}\theta}\right)^2}\,\mathrm{d}s = \int_0^\theta \sqrt{\left(r_0 + \frac{D}{2\pi}s\right)^2 + \left(\frac{D}{2\pi}\right)^2}\,\mathrm{d}s \\ &= \frac{1}{2}\left(\frac{2\pi}{D}\right)\left[\left(r_0 + \frac{D}{2\pi}\theta\right)\sqrt{\left(r_0 + \frac{D}{2\pi}\theta\right)^2 + \left(\frac{D}{2\pi}\right)^2}\right. \\ &\quad \left. - r_0\sqrt{r_0^2 + \left(\frac{D}{2\pi}\right)^2}\right] \\ &\quad + \frac{1}{2}\left(\frac{D}{2\pi}\right)\ln\left[\frac{\left(r_0 + \frac{D}{2\pi}\theta\right) + \sqrt{\left(r_0 + \frac{D}{2\pi}\theta\right)^2 + \left(\frac{D}{2\pi}\right)^2}}{r_0 + \sqrt{r_0^2 + \left(\frac{D}{2\pi}\right)^2}}\right]\end{aligned} \tag{3}$$

Equation (3) sows that ξ is a unique function of θ; therefore, at a fixed z, any variable defined on the spiral surface can be expressed as a function of the polar angle θ. Due to the small thicknesses of the Li-ion cell electrodes, it can be found that $(r_0 + (D/2\pi)\theta)^2$ is at least three orders larger than $(D/2\pi)^2$ for all θ, and Equation (3) can be approximated as:

$$\begin{aligned}\xi &= \int_0^\theta \sqrt{\left(r_0 + \frac{D}{2\pi}s\right)^2 + \left(\frac{D}{2\pi}\right)^2}\,\mathrm{d}s \approx \int_0^\theta \left(r_0 + \frac{D}{2\pi}s\right)\mathrm{d}s \\ &= r_0\theta + \frac{D}{4\pi}\theta^2\end{aligned} \tag{4}$$

therefore, an approximate functional relationship between θ and ξ can be derived from Equation (4):

$$\theta(\xi) \approx \frac{-r_0 + \sqrt{r_0^2 + \frac{D\xi}{\pi}}}{\frac{D}{2\pi}} \tag{5}$$

As shown in Equation (5), at a fixed z, any variable defined in the spiral surface can also be expressed as a function of the arc length ξ.

According to references [5–9], the current collector foils can be regarded as surfaces due to the small thickness, and the electrical potential of a current collector distributes only in the two tangential directions of the surface (ξ and z directions). Therefore, the charge balance equations on the current collector surfaces are:

$$\sigma_\mathrm{j}\frac{\partial^2\Phi_\mathrm{j}}{\partial\xi^2} + \sigma_\mathrm{j}\frac{\partial^2\Phi_\mathrm{j}}{\partial z^2} + i_{\mathrm{v,j}} = 0 \quad (\mathrm{j} = +, -) \tag{6}$$

where Φ_j is the electric potential of the current collector of electrode j, σ_j is the electric conductivity for the current collector of electrode j, and $i_{\mathrm{v,j}}$ is the volumetric current source in the current collector of electrode j. It can be found that Φ_j solved from Equation (6) is a function of ξ and z; therefore at a fixed z, Φ_j can be expressed as a function of the polar angle θ.

As discussed later in our work, certain electrical and thermal variables need to be evaluated along the spiral surface and extruded into the 3-D Cartesian coordinate system. The extrusion of variables can be performed through a coordinate transform algorithm. As shown in Fig. 1, $\psi'(\theta)$ is a variable defined on the spiral surface at a fixed z, and (x,y) is a specific Cartesian coordinate point which has the same z coordinate as $\psi'(\theta)$. Point (x,y) could be located either on or outside the spiral surface. The first step for variable extrusion is to project point (x,y) to the spiral surface along a specific direction defined by a ray from the origin and passing (x,y), the elevation angle θ_E (where $0 \le \theta_\mathrm{E} < 2\pi$) for the projecting direction can be calculated as follow:

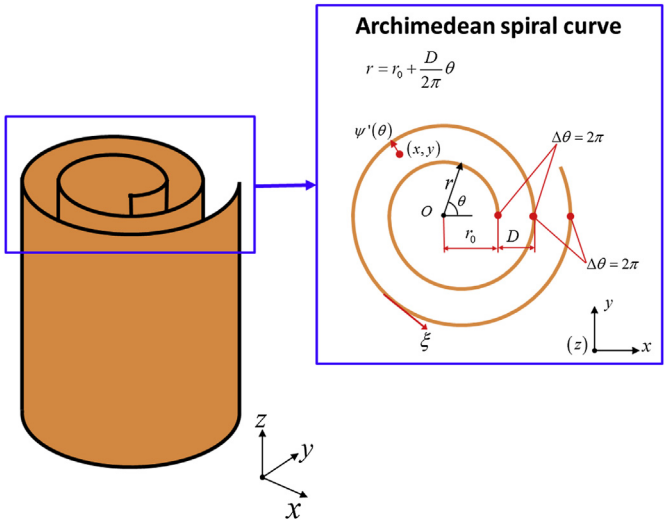

Fig. 1. Schematic for a surface wound through an Archimedean spiral locus.

$$\theta_E(x,y) = \begin{cases} \arccos\left(\frac{x}{\sqrt{x^2+y^2}}\right) & \text{if } y \geq 0 \\ 2\pi - \arccos\left(\frac{x}{\sqrt{x^2+y^2}}\right) & \text{if } y < 0 \end{cases} \quad (7)$$

The direction of projection is illustrated by the red (in the web version) arrow in Fig. 1 which can be approximately regarded as normal to the spiral surface. Next, define an integer n_w which defines an index for the nearest turning of the spiral surface to point (x,y):

$$n_w(x,y) = \left[\frac{\sqrt{x^2+y^2} - r_0 - \frac{D}{2\pi}\theta_E}{D}\right] \quad (8)$$

where the square brackets "[]" in this equation denote an operator to find the nearest integer to a real value. Thus, the polar angle for the projection of point (x,y) on the spiral surface can be calculated as:

$$\theta(x,y) = 2\pi \cdot n_w(x,y) + \theta_E(x,y) \quad (9)$$

Using Equation (9), a transform between the polar and Cartesian coordinates can be established:

$$\psi'(\theta) = \psi'(\theta(x,y)) = \psi''(x,y) \quad (10)$$

The algorithm described by Equations (7)–(10) shows that any variable evaluated on a spiral surface can be extruded to a Cartesian coordinate position in the space enclosed by the spiral surface.

The charge balance Equation (6) is defined on a 3-D spiral surface, but the dependent variables can be continuously distributed in the two tangential directions of the surface. Therefore, the computational domain for Equation (6) can be transformed into a 2-D flat surface (see Fig. 2), the ξ–z plane; the solutions for the charge balance are approximately same on both the spiral and the planar surfaces. This assertion will be validated later in this article.

2.2. The numerical difficulties for conventional modeling approaches

The configurations for a sector of the spirally-wound electrode pair in a jelly-roll are presented in Fig. 3, where the region inside the dashed box shows the array of layers intersecting a ray from the origin. As shown in Fig. 3, the parts between two adjacent opposite current collectors are defined as cell stacks and each cell stack includes a positive electrode coating layer, a separator layer, and a negative electrode coating layer. The electrical potentials of the current collectors are expressed as functions of polar angles; and the phrase "Stack(θ,θ')" stands for a cell stack in which the polar angles for the positive and negative electrode current collectors are respectively θ and θ' (where $\theta' = \theta$, $\theta + 2\pi$, or $\theta - 2\pi$). The symbol "$i_{N,(\theta,\theta')}$" denotes the transversal current density through the coating layers of stack (θ,θ').

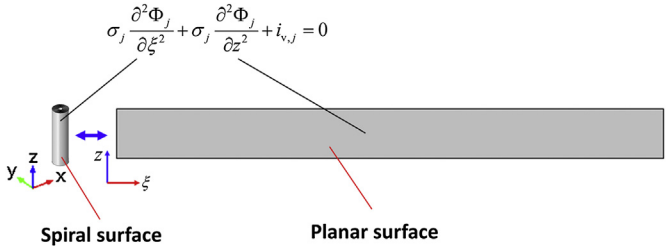

Fig. 2. Transform of computational domains for electrical equation for electrode j.

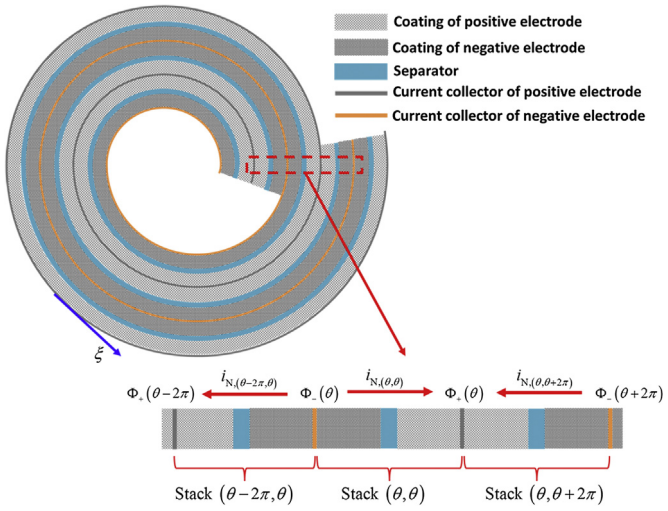

Fig. 3. Configuration for wound electrode pair.

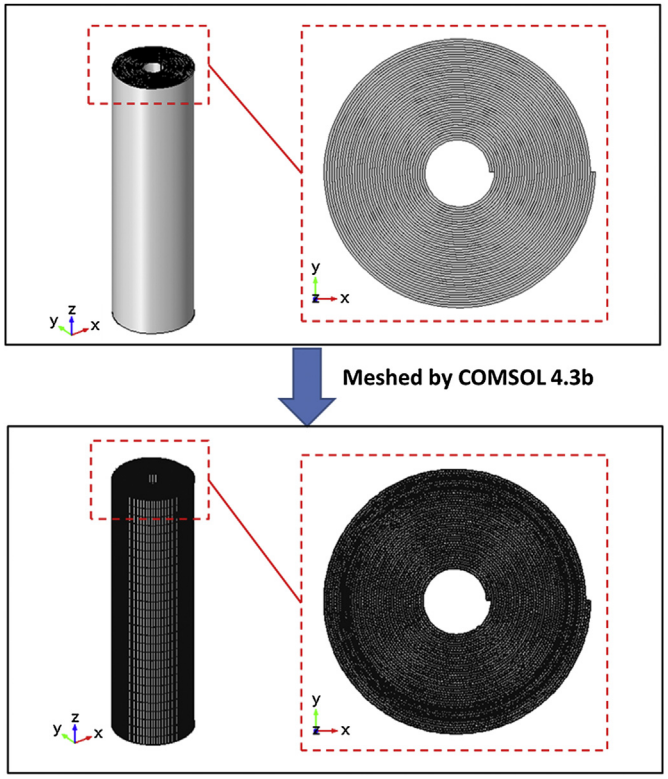

Fig. 4. Mesh pattern for the computation domains of jelly-roll where electrical insulation zones are included.

Fig. 3 shows that between two neighboring stacks, one of the two current collector potentials, Φ_+ or Φ_-, must be discontinuous; for example, from Stack($\theta - 2\pi$,θ) to Stack(θ,θ), the polar angle of Φ_+ jumps by 2π and therefore Φ_+ is discontinuous through these two stacks. However, the commonly-used numerical methods (finite element method, finite volume method, etc.) require all variables to be continuous in a mesh element. Therefore, if the charge balance Equation (6) is directly solved on the 3-D spiral surface, the maximum radial dimension for each mesh element must not exceed the thickness of a cell stack. Generally, the thickness of a cell stack is smaller than the dimensions of a jelly-roll by two orders of

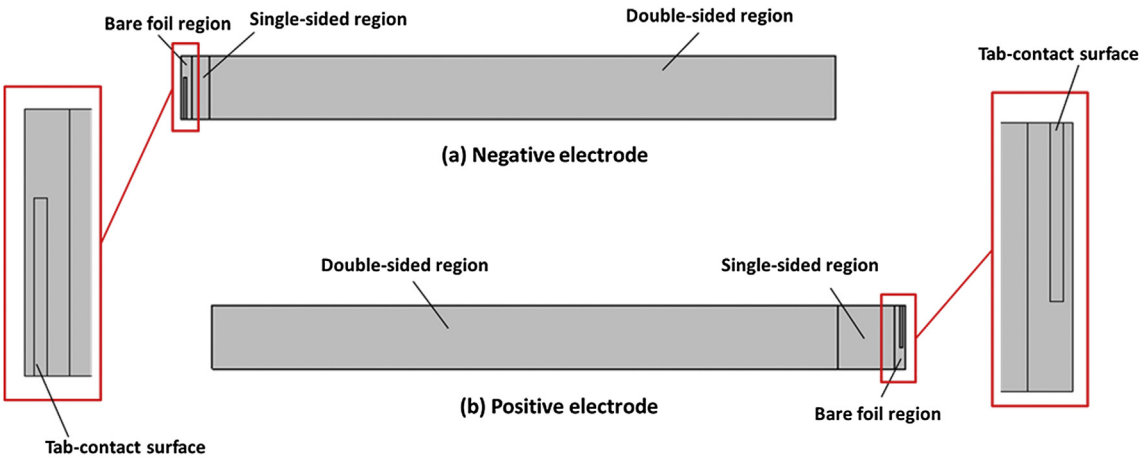

(a) Configuration of individual electrodes

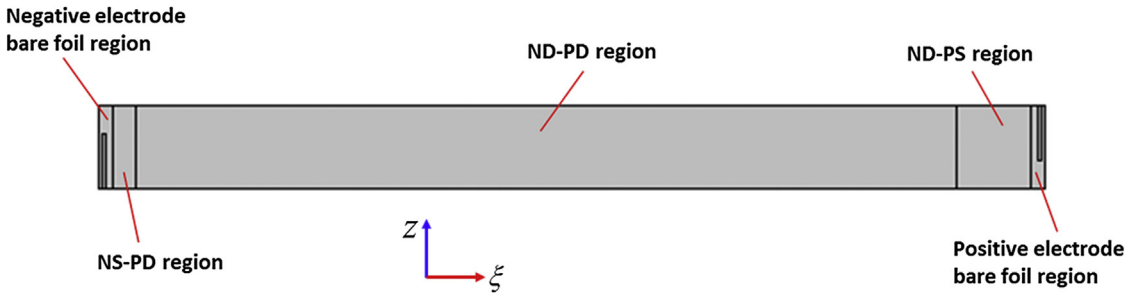

(b) Configuration of electrode pair

Fig. 5. The configurations for (a) individual electrodes, (b) electrode pair.

magnitude, and a very large number of mesh elements are required to ensure sufficient accuracy. Fig. 4 shows the mesh pattern for the modeling domain of a18650-type jelly-roll generated by COMSOL 4.3b. In the jelly-roll domain presented in Fig. 4, two 20-turn spiral surfaces are built as the electrical insulation interior boundaries, and a total of 511,241 domain elements are included to meet the default lowest mesh requirements by COMSOL, and this extremely fine mesh pattern would make the model computationally expensive.

2.3. Solutions for computation problems

Based on the ideas discussed in Section 2.1, we propose a new method which can greatly reduce the computational load for a 3-D spirally wound cell model. The electrical equation (6) is solved on a transformed 2-D planar domain for an electrode pair which is expressed as the ξ–z plane. The Joule heat source and the electrochemical heat source are also evaluated on the 2-D electrode pair domain and expressed as functions of θ and z; and these heat source terms are extruded to the jelly-roll domain built in the 3-D Cartesian coordinate system to be coupled with the 3-D thermal model.

2.4. The electrode configurations

Configurations for the two individual electrodes are presented in Fig. 5(a). Each electrode includes three different coating regions, the bare foil region where no coating is attached to the current collector foil, the single-sided region where only one side of the current collector has an active material coating, and the double-sided region where both sides of the current collector are coated. In the bare-foil region, there is a zone called the tab-contact surface on which the current enters/leaves the current collector form/to the external tabs. As shown in Fig. 5(b), by overlapping the coating regions of the two electrodes, the 2-D domain for electrode pair is obtained. In Fig. 5(b), the NS-PD region is the matching region for the single-sided negative electrode and the double-sided positive electrode, the ND-PD region is the matching region for the double-sided negative electrode and the double-sided positive electrode, and the ND-PS region is the matching region for the double-sided negative electrode and the single-sided positive electrode. The top-views for the matching of the coating regions in an electrode pair are presented in Fig. 6.

2.5. Electrochemical model for cell stacks

In this paper we have chosen to use an empirical equivalent circuit model [14] (ECM) to simulate the potential and current responses of each cell stack. According to reference 14, the equivalent circuit (see Fig. 7) includes two R–C branches ($R_p - C_p$ and $R_n - C_n$), a series resistor (R_s), and an open circuit voltage source (U). The governing equations and validation of the ECM are discussed in Appendix A.

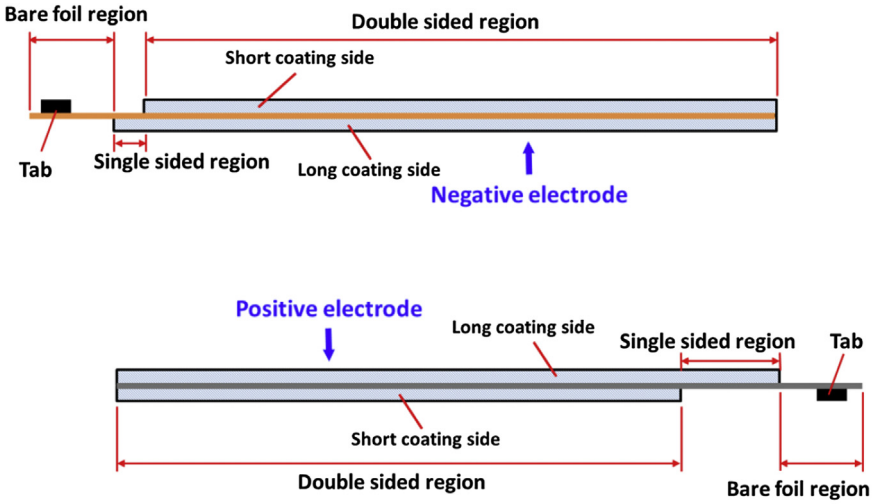

(a) Top-view for individual electrodes

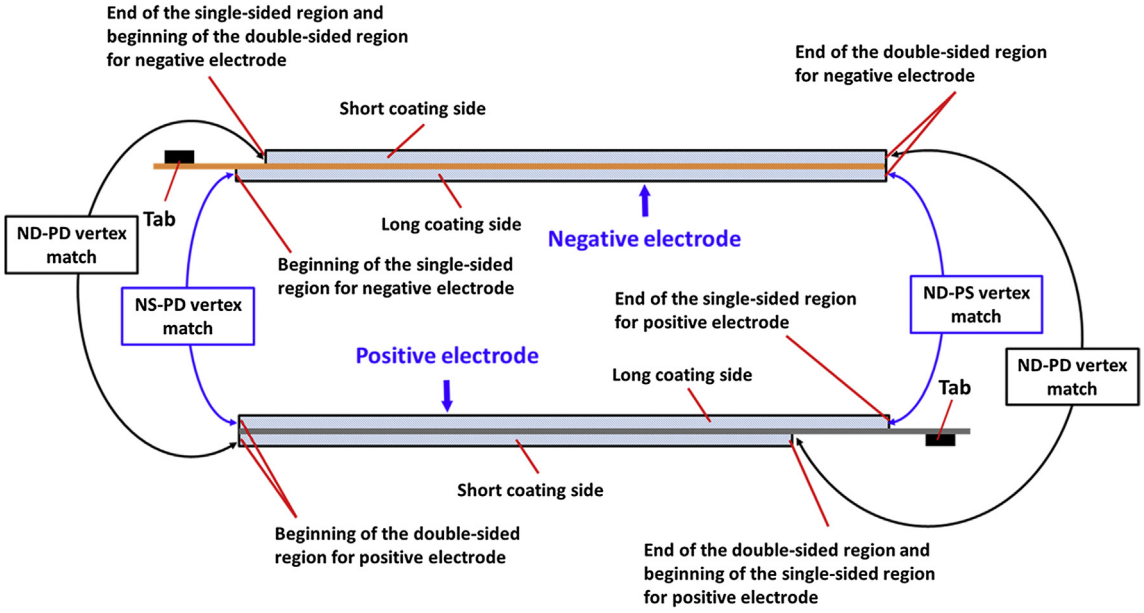

(b) The matching of coating layers in the electrode pair

Fig. 6. Top-views for the matching of coating regions in an electrode pair.

2.6. The current source terms

According to references [5–9], the volumetric current source in the current collectors, $i_{v,j}$ (j = +,−), are expressed by the transversal current density scaled by the thickness of current collector. Therefore, $i_{v,j}$ has a different expression in the different coating regions of the 2-D electrode pair domain presented in Fig. 5(b). The arrays of electrode component layers for the NS-PD, ND-PD, and ND-PS regions of a wound electrode pair are respectively presented in Fig. 8(a) through (c). Note that to make the illustrative schematics clear; the wound electrode pairs in Fig. 8 are presented as one-turn spirals, however, the practical jell-roll often has many more winding turns. In the NS-PD region shown in Fig. 8(a), the negative electrode current collector has only one side with the outward transversal current density and the positive electrode current collector has both sides with the inward transversal current

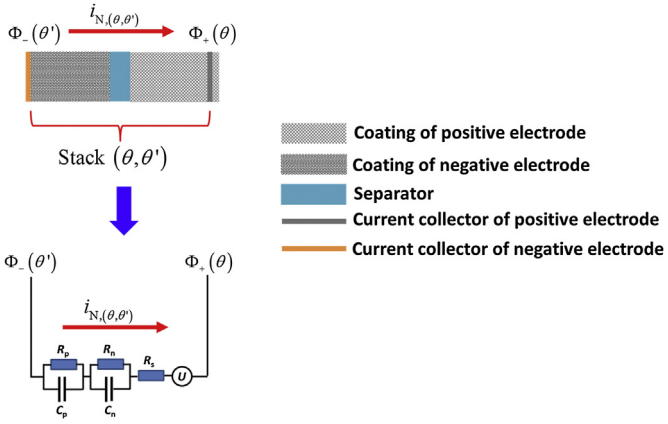

Fig. 7. Equivalent circuit for a cell stack.

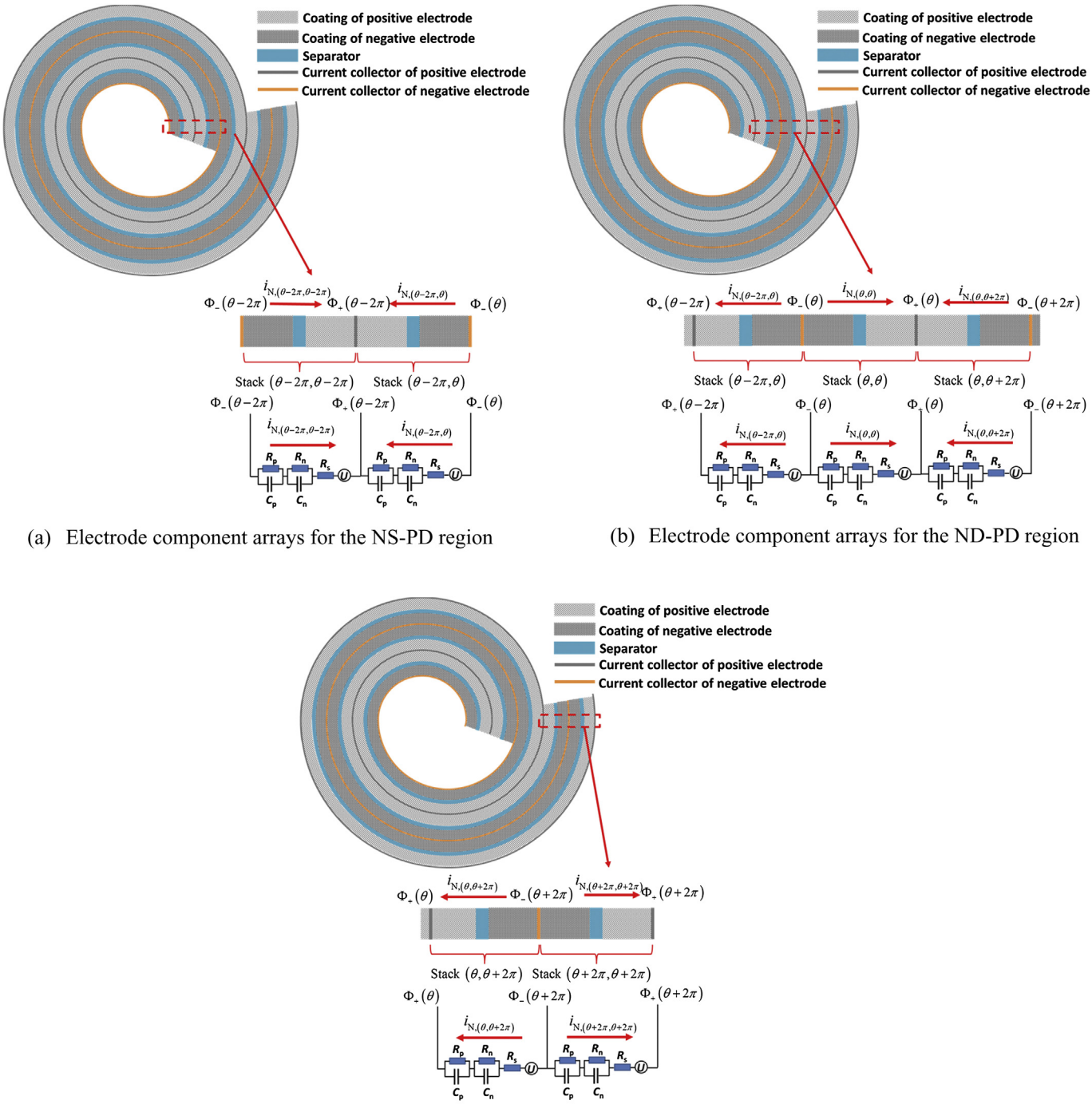

(a) Electrode component arrays for the NS-PD region

(b) Electrode component arrays for the ND-PD region

(c) Electrode component arrays for the ND-PS region

Fig. 8. The array patterns for electrode component layers in different coating regions: (a) for NS-PD region, (b) for ND-PD region, (c) for ND-PS region.

density; therefore, the volumetric current source terms at the polar angle $\theta_1 = \theta - 2\pi$ are expressed as:

$$i_{v,+}(\theta_1) = \frac{i_{N,(\theta_1,\theta_1)} + i_{N,(\theta_1,\theta_1+2\pi)}}{\delta_+} \tag{11}$$

$$i_{v,-}(\theta_1) = -\frac{i_{N,(\theta_1,\theta_1)}}{\delta_-} \tag{12}$$

where δ_+ and δ_- are respectively the thicknesses for the current collectors of positive and negative electrodes. In the ND-PD region shown in Fig. 8(b), the negative electrode current collector has both sides with the outward transversal current density and the positive electrode current collector has both sides with the inward transversal current density; therefore, the volumetric current source terms at the polar angle θ are expressed as:

$$i_{v,+}(\theta) = \frac{i_{N,(\theta,\theta)} + i_{N,(\theta,\theta+2\pi)}}{\delta_+} \tag{13}$$

$$i_{v,-}(\theta) = -\frac{i_{N,(\theta-2\pi,\theta)} + i_{N,(\theta,\theta)}}{\delta_-} \tag{14}$$

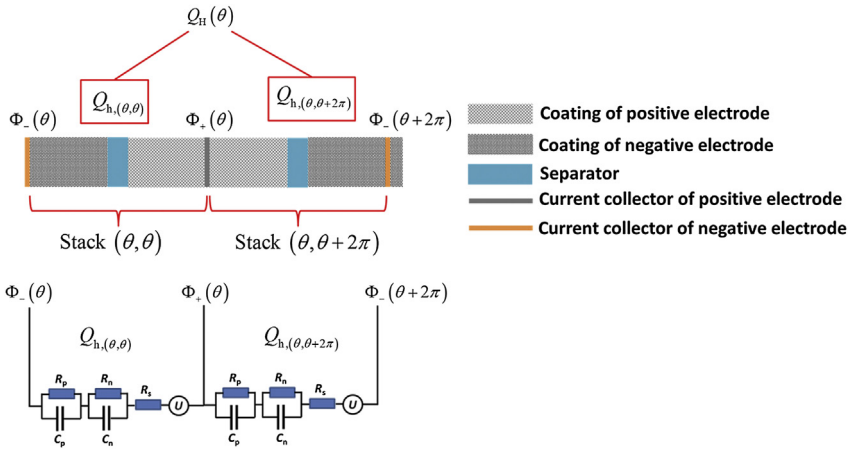

Fig. 9. Definition of the average heat generation rate for two neighboring cell stacks.

In the ND-PS region shown in Fig. 8(c), the negative electrode current collector has both sides with the outward transversal current density and the positive electrode current collector has only one side with the inward transversal current density; therefore, the volumetric current source terms at the polar angle $\theta_2 = \theta + 2\pi$ are expressed as:

$$i_{v,+}(\theta_2) = \frac{i_{N,(\theta_2,\theta_2)}}{\delta_+} \tag{15}$$

$$i_{v,-}(\theta_2) = -\frac{i_{N,(\theta_2-2\pi,\theta_2)} + i_{N,(\theta_2,\theta_2)}}{\delta_-} \tag{16}$$

In the tab-contact surfaces of the bare-foil regions, the current source terms are expressed as:

$$i_{v,+} = \frac{I_{App}}{A_+\delta_+} \tag{17}$$

$$i_{v,-} = -\frac{I_{App}}{A_-\delta_-} \tag{18}$$

where A_+ and A_- are the area of the tab-contact surfaces for the positive and negative electrodes, and I_{App} is the applied current on the cell which is defined as positive for charge and negative for discharge. The current source is zero at other positions in the bare-foil regions.

2.7. The heat source terms

According to the equivalent circuit model, the volume-average electrochemical heat through the thickness of the cell stack in Fig. 7 can be calculated as:

$$Q_{EC,(\theta,\theta')} = -\frac{i_{N,(\theta,\theta')}\left[\Phi_+(\theta) - \Phi_-(\theta') - U\right]}{\delta_s} \tag{19}$$

where δ_s is the thickness for a cell stack. The volume-average Joule heat through the cell stack is expressed as:

$$Q_{J,(\theta,\theta')} = \frac{0.5\delta_+\sigma_+}{\delta_s}\left[\left(\frac{\partial\Phi_+}{\partial\xi}\Big|_\theta\right)^2 + \left(\frac{\partial\Phi_+}{\partial z}\Big|_\theta\right)^2\right] + \frac{0.5\delta_-\sigma_-}{\delta_s}\left[\left(\frac{\partial\Phi_-}{\partial\xi}\Big|_{\theta'}\right)^2 + \left(\frac{\partial\Phi_-}{\partial z}\Big|_{\theta'}\right)^2\right] \tag{20}$$

and the total heat generation rate throughout cell stack (θ,θ') is:

$$Q_{h,(\theta,\theta')} = Q_{EC,(\theta,\theta')} + Q_{J,(\theta,\theta')} \tag{21}$$

The average heat generation rate (see Fig. 9) for the two adjacent cell stacks which share the same positive electrode current collector is obtained as a unique function of polar angle θ:

$$Q_H(\theta) = \frac{Q_{h,(\theta,\theta)} + Q_{h,(\theta,\theta+2\pi)}}{2} \tag{22}$$

Table 1
Expressions for volumetric current source and heat generation rates in different coating regions.

Coating regions	Current source terms	Heat source terms
Bare-foil region for negative electrode	$i_{v,-}(\theta) = -\frac{I_{App}}{A_-\delta_-}$ (tab-contact − surface) $i_{v,-}(\theta) = 0$ (other locations)	$Q_H(\theta) = \sigma_-\left[\left(\frac{\partial\Phi_-}{\partial\xi}\Big\|_\theta\right)^2 + \left(\frac{\partial\Phi_-}{\partial z}\Big\|_\theta\right)^2\right]$
NS-PD region	$i_{v,+}(\theta) = \frac{i_{N,(\theta,\theta)}+i_{N,(\theta,\theta+2\pi)}}{\delta_+}$ $i_{v,-}(\theta) = -\frac{i_{N,(\theta,\theta)}}{\delta_-}$	$Q_H(\theta) = \frac{Q_{h,(\theta,\theta)}+Q_{h,(\theta,\theta+2\pi)}}{2}$
ND-PD region	$i_{v,+}(\theta) = \frac{i_{N,(\theta,\theta)}+i_{N,(\theta,\theta+2\pi)}}{\delta_+}$ $i_{v,-}(\theta) = -\frac{i_{N,(\theta-2\pi,\theta)}+i_{N,(\theta,\theta)}}{\delta_-}$	$Q_H(\theta) = \frac{Q_{h,(\theta,\theta)}+Q_{h,(\theta,\theta+2\pi)}}{2}$
ND-PS region	$i_{v,+}(\theta) = \frac{i_{N,(\theta,\theta)}}{\delta_+}$ $i_{v,-}(\theta) = -\frac{i_{N,(\theta-2\pi,\theta)}+i_{N,(\theta,\theta)}}{\delta_-}$	$Q_H(\theta) = Q_{h,(\theta,\theta)}$
Bare-foil region for positive electrode	$i_{v,+}(\theta) = \frac{I_{App}}{A_+\delta_+}$ (tab-contact − surface) $i_{v,+}(\theta) = 0$ (other locations)	$Q_H(\theta) = \sigma_+\left[\left(\frac{\partial\Phi_+}{\partial\xi}\Big\|_\theta\right)^2 + \left(\frac{\partial\Phi_+}{\partial z}\Big\|_\theta\right)^2\right]$

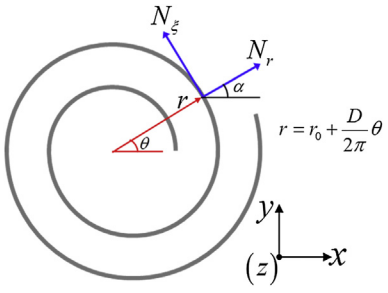

Fig. 10. Schematic for the directions of heat fluxes in a jelly-roll.

Note that in the ND-PS region, the positive electrode current collector is single-sided and the expression for the heat generation rate is as follow:

$$Q_H(\theta) = Q_{h,(\theta,\theta)} \tag{23}$$

In the bare-foil regions, the electrochemical heat is zero and the heat generation rates only include the Joule heat; therefore for the positive electrode

$$Q_H(\theta) = \sigma_+\left[\left(\frac{\partial\Phi_+}{\partial\xi}\Big|_\theta\right)^2 + \left(\frac{\partial\Phi_+}{\partial z}\Big|_\theta\right)^2\right] \tag{24}$$

and for the negative electrode

$$Q_H(\theta) = \sigma_-\left[\left(\frac{\partial\Phi_-}{\partial\xi}\Big|_\theta\right)^2 + \left(\frac{\partial\Phi_-}{\partial z}\Big|_\theta\right)^2\right] \tag{25}$$

The expressions for the volumetric current sources and heat generation rates in different coating regions are summarized in Table 1.

2.8. Thermal model

Since all of the electrode component layers are thermally conductive, the heat fluxes in the jelly-roll are continuous in all three directions; therefore, the thermal model must be solved in a 3-D computational domain. The governing equation for the thermal model is as follow:

$$\rho C_P\frac{\partial T}{\partial t} = \nabla\cdot\left(\underline{\underline{\mathbf{k}}}\nabla T\right) + Q''_H \tag{26}$$

where ρ is the density of the jelly-roll, C_P is the specific heat capacity of the jelly-roll, $\underline{\underline{\mathbf{k}}}$ is the matrix for the anisotropic thermal conductivity of the jelly-roll, and Q''_H is the extruded volumetric heat source in the 3-D Cartesian coordinate system in the jelly-roll.

In a jelly-roll, the electrode component layers are arrayed in series along the normal direction of the spiral surface and in parallel along the tangential direction of the spiral surface. Due to such an array pattern, the thermal conductivity of the jelly-roll has different values in the tangential and normal directions of the spiral surface. As shown in Fig. 10, at a location with polar angle θ, N_ξ denotes the heat flux along the tangential direction of the spiral surface, N_r denotes the heat flux along the normal direction from the spiral surface, and the value for θ can be determined from the Cartesian coordinates using Equations (7)–(9). The angle between the normal direction of the spiral surface and the x axis, α, can be derived as:

$$\alpha = \theta + \arctan\left(2\pi\frac{r}{D}\right) - \frac{\pi}{2} \tag{27}$$

The expressions for N_ξ and N_r in the Cartesian coordinate system are as follow:

$$N_\xi = -k_\xi\frac{\partial T}{\partial\xi} = -k_\xi\left(-\sin\alpha\frac{\partial T}{\partial x} + \cos\alpha\frac{\partial T}{\partial y}\right) \tag{28}$$

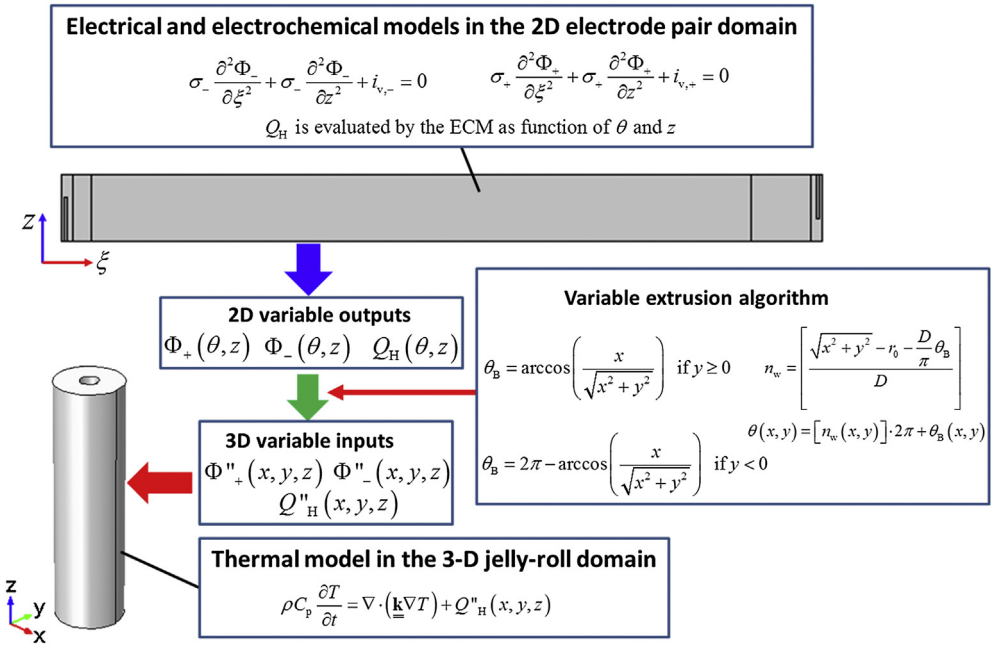

Fig. 11. Flowchart for the solution procedure using our proposed algorithm.

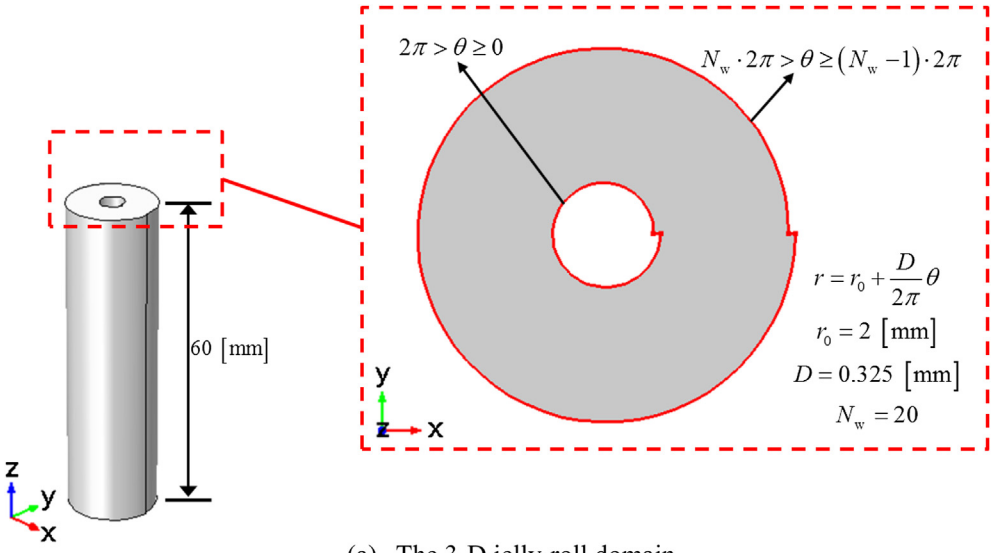

(a) The 3-D jelly-roll domain

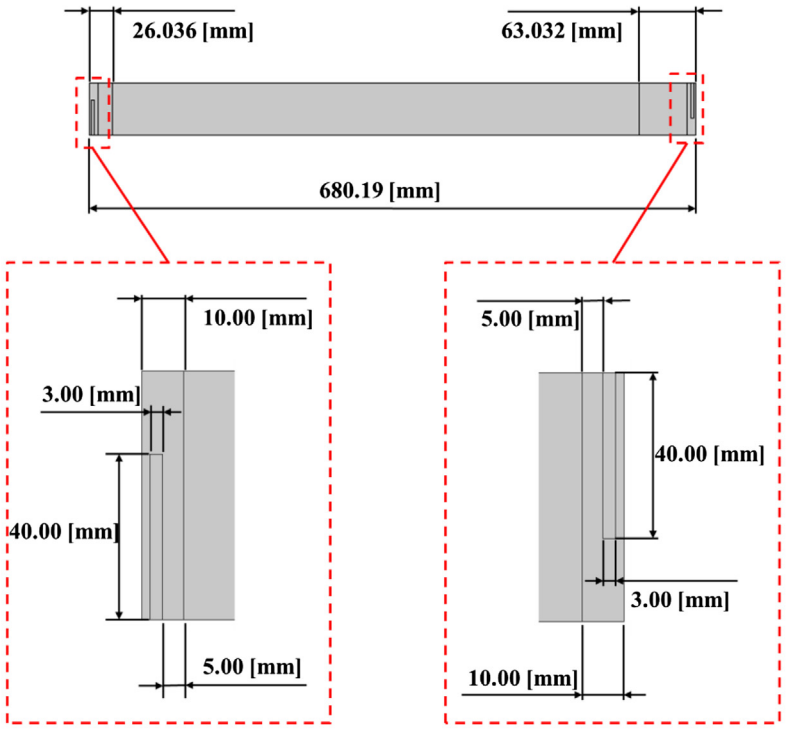

(b) The 2-D electrode pair domain

Fig. 12. Computational domains for our jelly-roll model: (a) 3-D jelly-roll domain, (b) 2-D electrode pair domain.

$$N_r = -k_r \frac{\partial T}{\partial r} = -k_r \left(\cos\alpha \frac{\partial T}{\partial x} + \sin\alpha \frac{\partial T}{\partial y} \right) \tag{29}$$

where k_ξ and k_r are respectively the thermal conductivities in the tangential and normal directions of the spiral surface. The heat fluxes in the x, y, and z directions can be expressed as:

$$\begin{aligned} N_x &= \cos\alpha N_r - \sin\alpha N_\xi \\ &= -\left(k_r \cos^2\alpha + k_\xi \sin^2\alpha \right) \frac{\partial T}{\partial x} - \left(k_r - k_\xi \right) \sin\alpha\cos\alpha \frac{\partial T}{\partial y} \end{aligned} \tag{30}$$

$$\begin{aligned} N_y &= \sin\alpha N_r + \cos\alpha N_\xi \\ &= -\left(k_r - k_\xi \right) \sin\alpha\cos\alpha \frac{\partial T}{\partial x} - \left(k_r \sin^2\alpha + k_\xi \cos^2\alpha \right) \frac{\partial T}{\partial y} \end{aligned} \tag{31}$$

$$N_z = -k_\xi \frac{\partial T}{\partial z} \tag{32}$$

Equations (30)–(32) can be expressed in vector-matrix format:

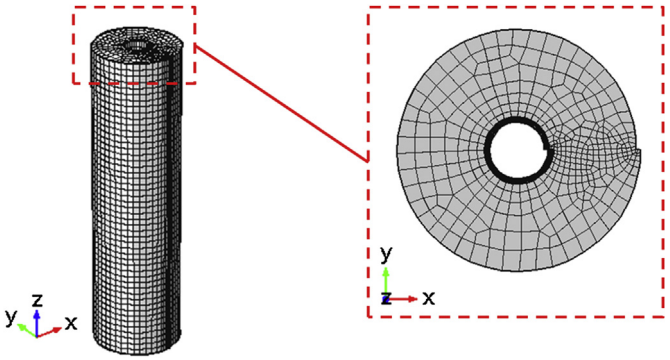

Fig. 13. Mesh pattern for the 3-D jelly-roll domain.

Table 2
Values of parameters.[a]

Symbol	Value	Unit
C	1.17	Ah
C_P	750	J K^{-1} kg^{-1}
D	3.25×10^{-4}	m
i_C	15	A m^{-2}
k_r	0.8	W K^{-1} m^{-1}
k_ξ	30	W K^{-1} m^{-1}
N_w	20	
r_0	2×10^{-3}	m
δ_+	20×10^{-6}	m
δ_-	15×10^{-6}	m
δ_s	1.625×10^{-4}	m
ρ	2720	kg m^{-3}
σ_+	3.8×10^7	S m^{-1}
σ_-	6.33×10^7	S m^{-1}

[a] Parameters are obtained from Ref. [7] and scaled to the cell size in this article.

$$\begin{bmatrix} N_x \\ N_y \\ N_z \end{bmatrix} = -\begin{bmatrix} k_r\cos^2\alpha + k_\xi\sin^2\alpha & \left(k_r - k_\xi\right)\sin\alpha\cos\alpha & 0 \\ \left(k_r - k_\xi\right)\sin\alpha\cos\alpha & k_r\sin^2\alpha + k_\xi\cos^2\alpha & 0 \\ 0 & 0 & k_\xi \end{bmatrix}\begin{bmatrix} \frac{\partial T}{\partial x} \\ \frac{\partial T}{\partial y} \\ \frac{\partial T}{\partial z} \end{bmatrix} \tag{33}$$

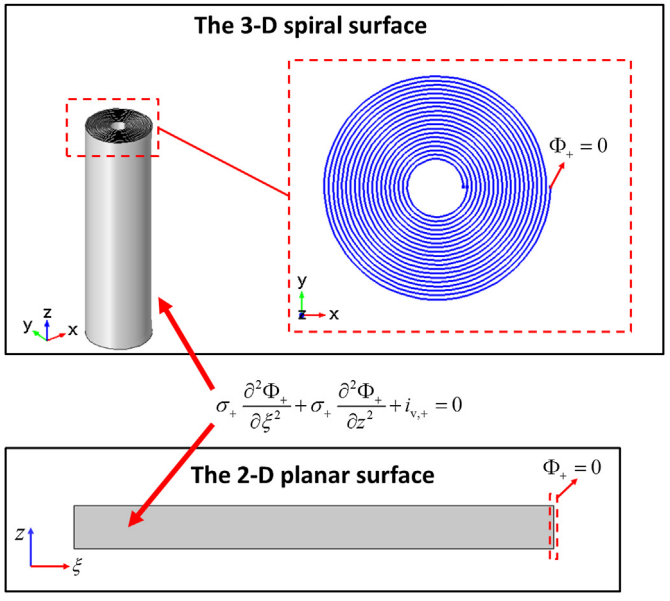

Fig. 14. Computational domains for validating the coordinate transform algorithm.

therefore, the elements of $\underline{\underline{\mathbf{k}}}$ can be obtained from Equation (33):

$$\underline{\underline{\mathbf{k}}} = \begin{bmatrix} k_r\cos^2\alpha + k_\xi\sin^2\alpha & \left(k_r - k_\xi\right)\sin\alpha\cos\alpha & 0 \\ \left(k_r - k_\xi\right)\sin\alpha\cos\alpha & k_r\sin^2\alpha + k_\xi\cos^2\alpha & 0 \\ 0 & 0 & k_\xi \end{bmatrix} \tag{34}$$

2.9. Solution procedure

A flowchart for the solution procedure using our coordinate transform and variable extrusion methods is presented in Fig. 11. The charge balance equations and the electrochemical model are solved in the transformed 2-D domain for the electrode pair, and the volumetric heat source term Q_H is evaluated as a function of polar angle θ and z using Equations (19)–(25). Then $Q_H(\theta,z)$ is transformed as a function of Cartesian coordinates, $Q''_H(x,y,z)$, and extruded to the 3-D jelly-roll domain using the algorithm described by Equations (7)–(9). The thermal model is coupled with the extruded heat source term and solved in the 3-D jelly-roll domain. The two electrical potentials, Φ_+ and Φ_-, are also extruded to check the accuracy of our algorithms. It is noted that the variables extruded from the 2-D domain to the 3-D domain must be explicit expressions of the coordinates, and the solutions for this issue are discussed in Appendix B.

The geometries for the two computational domains are presented in Fig. 12, the 3-D domain for a twenty-turn jelly-roll is regarded as a continuous phase enclosed by two spiral surfaces following the polar equation (1). For the interior surface, the polar angle, θ, changes from 0 to 2π; for the exterior surface, θ changes from $(N_w - 1)2\pi$ to $N_w 2\pi$, where $N_w = 20$ is the number of turns for the wound electrodes.

Using the numerical procedure presented in Fig. 11, only Equation (26) is solved in a 3-D domain where the fluxes are continuous in all directions, there is no need to define the insulated interior boundaries in the 3-D domain, and the meshing requirements are greatly lowered. Fig. 13 shows the mesh pattern for the 3-D jelly-roll domain as our method is applied, only 21,950 domain elements are included, and the computational load is significantly reduced compared to the model with the mesh shown in Fig. 4.

3. Results and discussion

The mathematical model developed in Section 2 was implemented using COMSOL Multi-physics 4.3b with the parameter values listed in Table 2.

3.1. Validation of the coordinate transform method

To validate our method for the coordinate transformation, we need to show that Equation (6) solved on a 3-D spiral surface and on a 2-D plane have the same solution. In this case, we segregated the charge balance equation for the positive electrode current collector by setting the volumetric current source as a constant which is equivalent to 5C discharge:

$$i_{v,+} = 5\frac{i_C}{0.5\delta_+} \tag{35}$$

where i_C is the transversal current density for C rate. As shown in Fig. 14, a twenty-turn spiral surface was built in the 3-D Cartesian coordinate system; a rectangular domain was built in the $\xi - z$ plane, the height of the rectangular domain is same with that of the spiral surface and the span of the rectangular in the ξ direction equals the

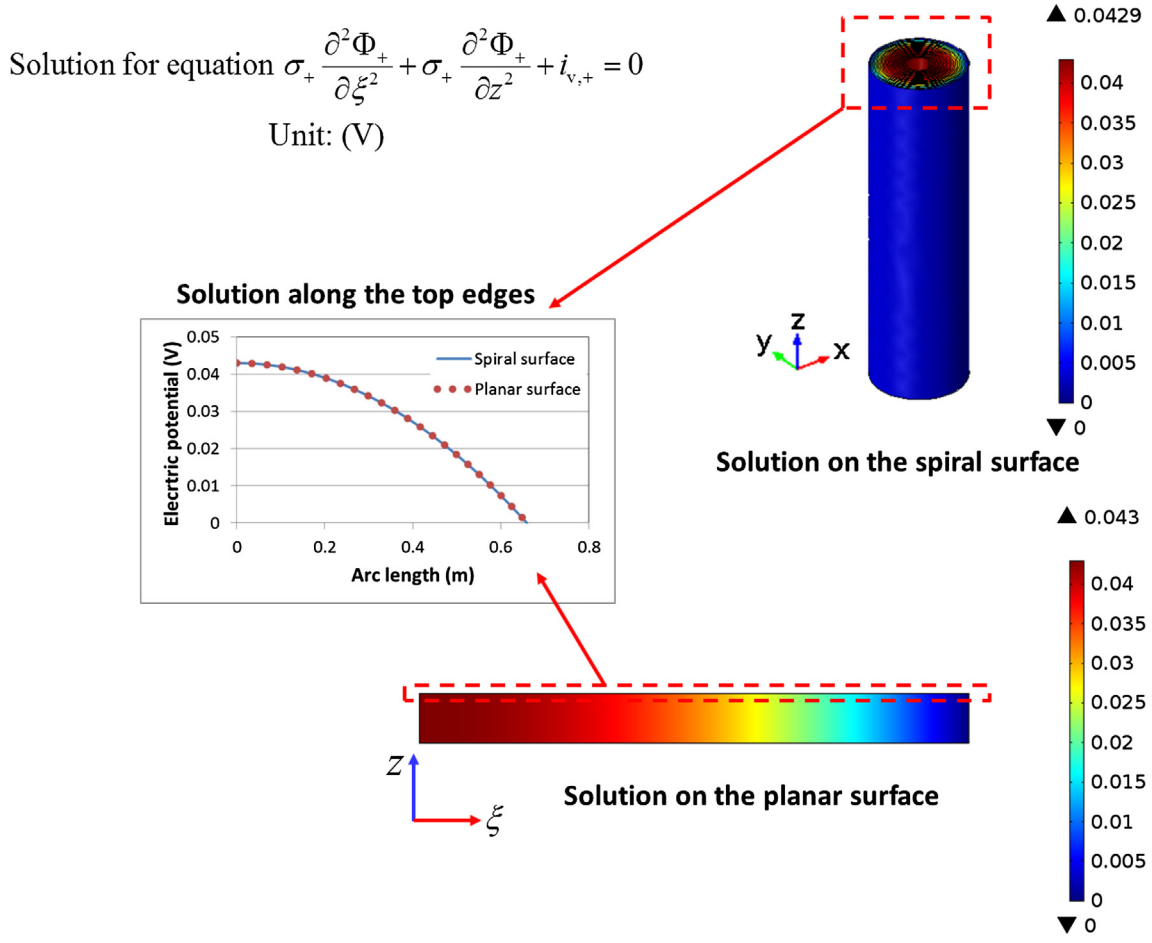

Fig. 15. Solutions for electrical equation solved on spiral and planar surfaces.

tangential arc length of the spiral surface. The boundary conditions are $\Phi_+ = 0$ for the exterior edge of the spiral surface and the right edge of the rectangular domain. With a constant current source, the charge balance equation is steady-state. The results from the spiral and planar surfaces are presented in Fig. 15, and there is perfect agreement between the solutions from the two computational domains.

3.2. Validation of the variable extrusion algorithm

The variable extrusion algorithm (see Equation (10)) was validated using the results from a simulated 5C discharge, and the purpose was to check agreement between a variable in the 2-D domain and its extrusion in the 3-D domain. It is the volumetric heat source, Q_H, that couples the 2-D electrical equations and the 3-D thermal equations, therefore, the Q_H values evaluated in the 2-D electrode pair domain and extruded to the 3-D jelly-roll domain at the beginning and end of 5C discharge are presented in Fig. 16. As shown in Fig. 16, the heat source is higher in the tab-contact surfaces of the two electrodes due to the large current density, and the good agreement between 2-D and 3-D values confirms the high accuracy of the variable extrusion algorithm.

To further clarify the strength of this algorithm, the Q_H vs time plots at different mapped point pairs are presented in Fig. 17. A mapped point pair includes a 2-D point i with coordinates (ξ,z) and a 3-D point i'' with coordinates (x,y,z), where x, y, and ξ satisfy the relations presented in Equations (3) and (7)–(9). The 2-D and 3-D coordinates for the three mapped point pairs selected at different coating regions are listed in Table 3. As shown in Fig. 17, the heat source values in the NS-PD (mapped point pair 1) and ND-PS (mapped point pair 3) regions are higher than those in the ND-PD (mapped point pair 2) region; the reason is that the NS-PD and ND-PS regions are located closer to the tab-contact surfaces. The major cause for the error between the 2-D and 3-D values is the approximation approach presented in Appendix B, and the accuracy of the variable extrusion between the 2-D and 3-D domains could be improved by including more nodes or using higher order basis functions in the approximate expressions of the variables. The 2-D and 3-D plots of the current collector potentials for the positive and negative electrodes at the end of 5C discharge are presented in Fig. 18; and the results also show good accuracy in the 2-D to 3-D variable extrusion.

3.3. Thermal case studies

The simulated temperature profiles at the end of 1C, 3C, and 5C discharges are presented in Fig. 19, where the initial and ambient temperatures are set at 25 °C and the convective heat transfer coefficient at the exterior spiral surface, h, is set as 1.0 W m^{-2} K^{-1}. As shown in all the three plots, there are hot regions located at the outer surface and near the end of the winding turn, which are corresponding to the higher heat generation rates in the tab-contact surface of the positive electrode.

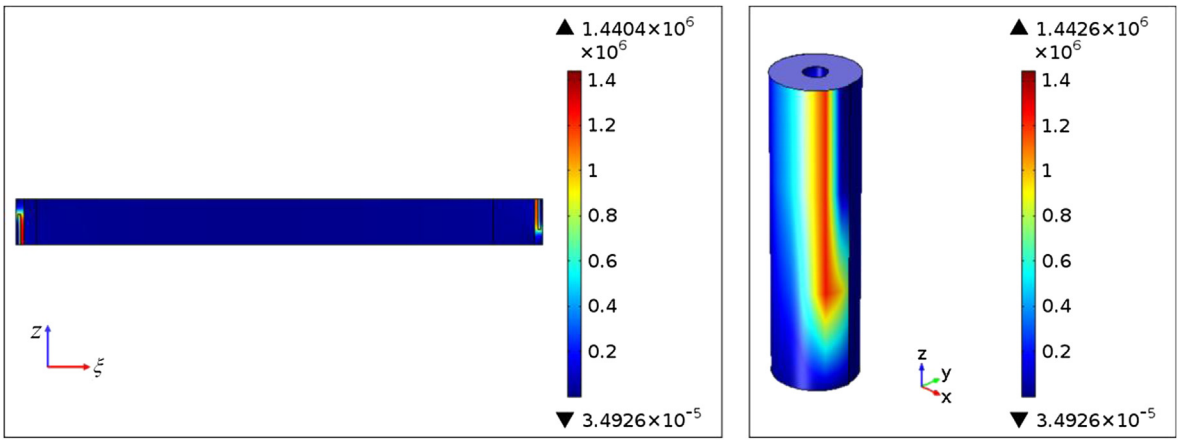

(a) Heat generation rate at the beginning of 5C discharge

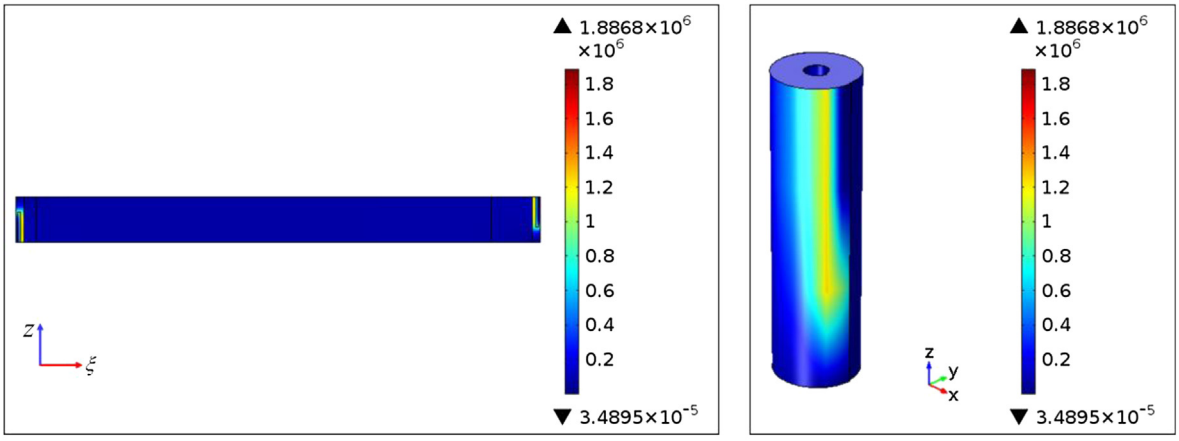

(b) Heat generation rate at the end of 5C discharge

Fig. 16. Profiles for heat generation rates (in W m^{-3}) in 2-D and 3-D domains at the beginning and end of 5C discharge.

The effects of thermal boundary conditions on the temperature profiles are also discussed. The distributed thermal results at the end of 5C discharge with $h = 1.0$ W m^{-2} K^{-1} and $h = 10.0$ W m^{-2} K^{-1} are presented in Fig. 20. According to Fig. 20, the temperature of the jelly-roll decreases by about 8 °C when the value of h increases from 1 to 10 W m^{-2} K^{-1}; and at high convection rate, the temperature difference between the center and outer surfaces of the jelly-roll becomes larger and the temperature of the outer surface drops more rapidly than the center surface.

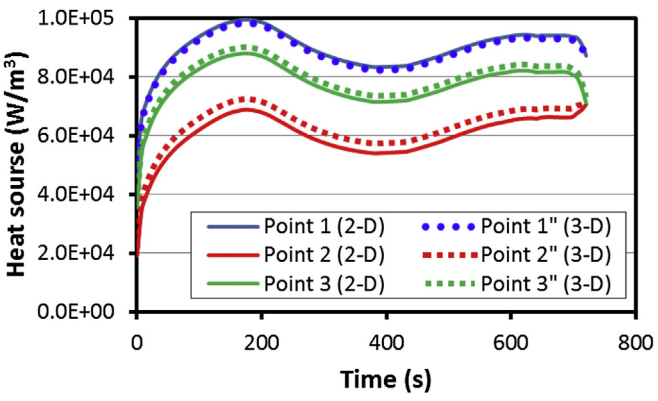

Fig. 17. Change of heat generation rates at different mapped point pairs over time.

3.4. Comparisons between our method and conventional method

As discussed in Section 2.2, in a conventional way, the electrical, electrochemical, and thermal models can be solved in an extremely fine meshed 3-D domain (Fig. 4). However, running such a coupled multi-physics model exceeds the memory limitations for most PCs. For this reason, we present comparisons based on a segregated thermal model; that is, the heat source term is set as a constant (i.e. 1×10^5 W m^{-3}) and thus independent of the electrochemical and

Table 3
2-D and 3-D coordinates for different mapped point pairs.

	x [m]	y [m]	z [m]	ξ [m]	Region
Mapped point pair 1	0	0.025	0.01	0.01858	NS-PD
Mapped point pair 2	0	0.05	0.03	0.21307	ND-PD
Mapped point pair 3	0	0.082	0.03	0.63994	ND-PS

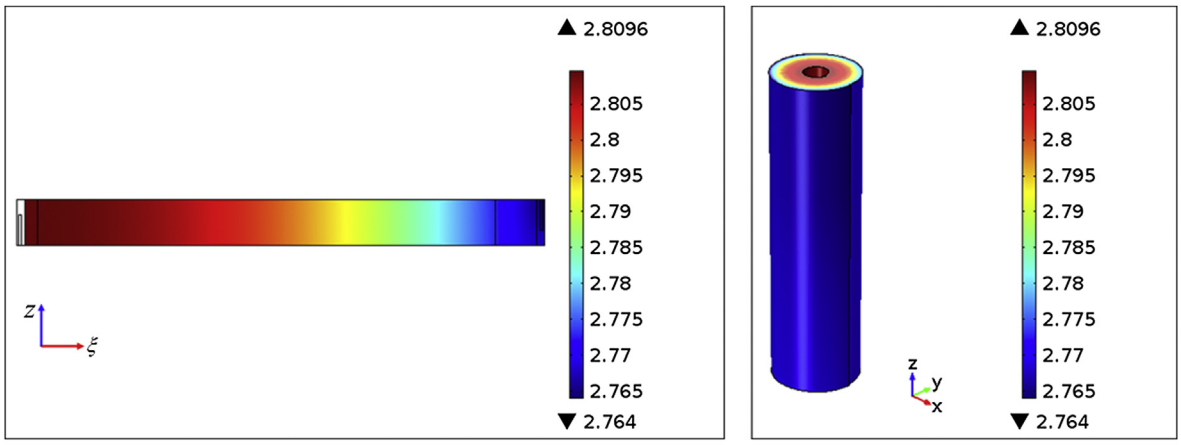

(a) Electrical potential for positive electrode current collector

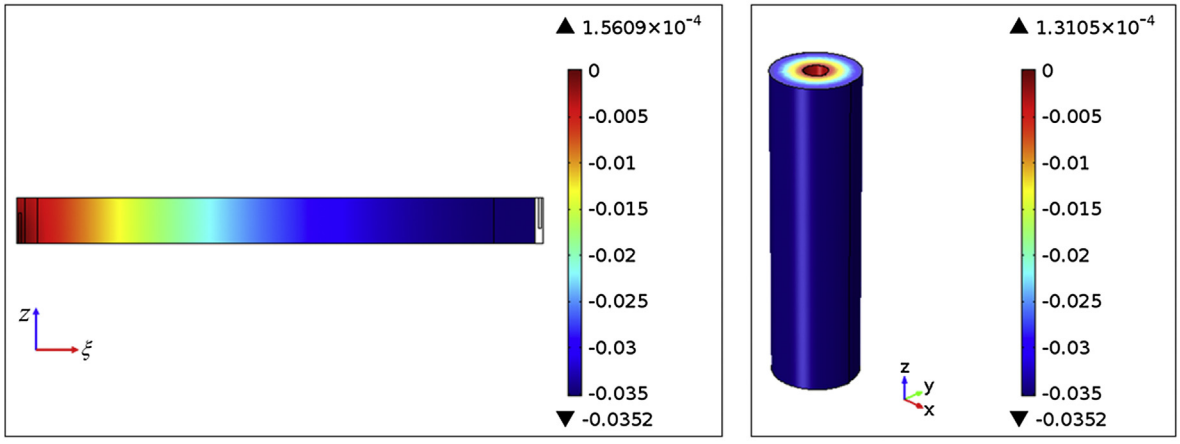

(b) Electrical potential for negative electrode current collector

Fig. 18. Profiles for electrical potentials (in V) of current collectors in 2-D and 3-D domains at the end of 5C discharge.

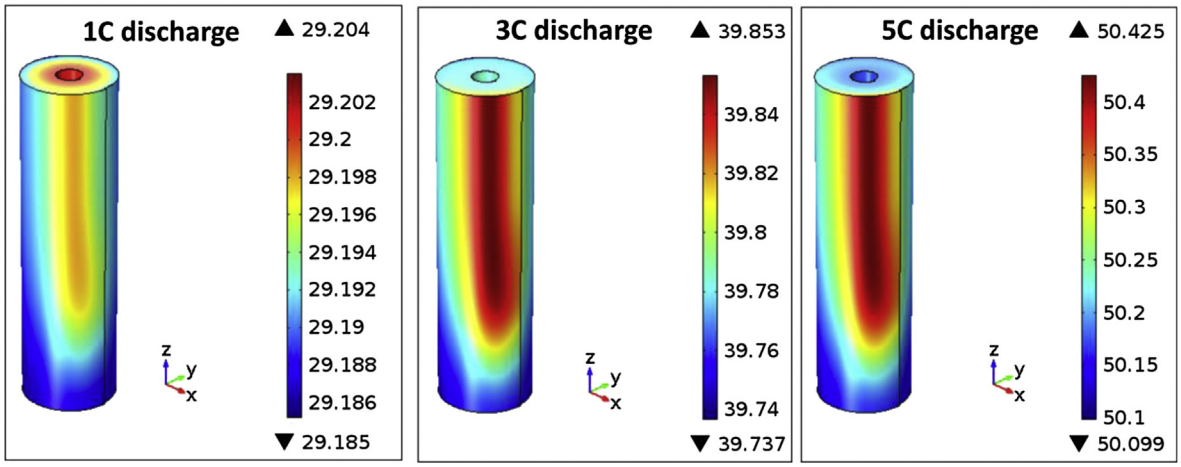

Fig. 19. Profiles for jelly-roll temperature (in °C) at the end of 1C, 3C, and 5C discharges.

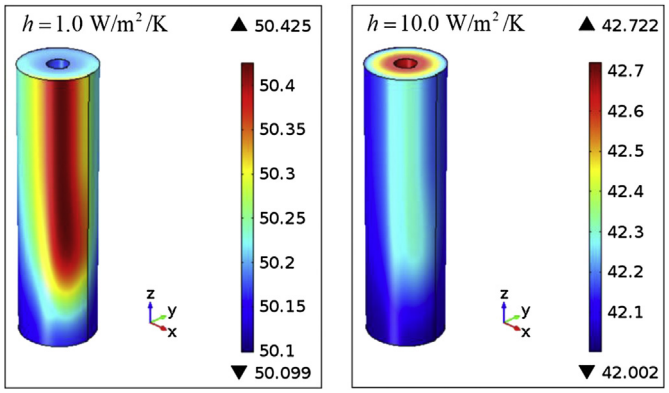

Fig. 20. Profiles for jelly-roll temperature (in °C) at the end of 5C discharges with different heat transfer coefficients.

electrical models. As shown in Fig 21(a), for the conventional method, the thermal model is directly solved in the extremely-fine-mesh domain where the 3-D heat source term, $Q''_H(x,y,z)$, is set equal to constant. As shown in Fig. 21(b), using our method, the heat source term is defined as a constant in the 2-D electrode pair domain and extruded using the algorithm developed in this article to a coarsely meshed 3-D domain where the thermal model is solved. The solutions for thermal model obtained by the two methods are exactly same as shown in Fig. 21. By the conventional way, it takes 1 h 55 min and 11.1GB physical memory for the PC to compute the results; however, with our method, it takes only 3 min 54 s and 3.8 GB physical memory.

If the electrical and electrochemical models are included, these additional models would be solved in the extremely-fine-mesh 3-D domain for conventional methods, but in the coarsely-meshed 2D domain for our method. Based on the above discussions, we can

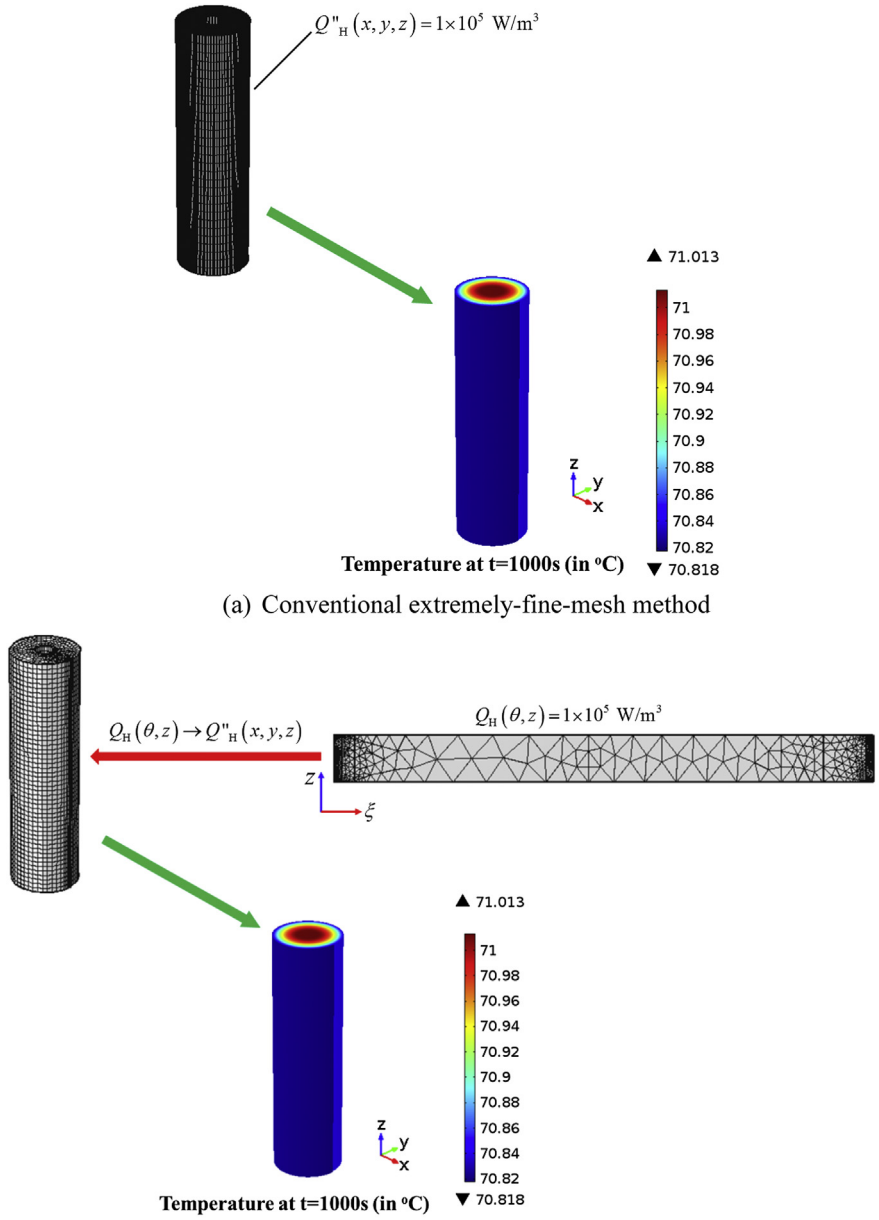

Fig. 21. Solving a segregated thermal model using (a) conventional extremely-fine-mesh method (b) coordinate transform and variable extrusion method.

conclude that our method would be advantageous for solving the coupled models.

4. Conclusion

In this article, a numerical method is presented to reduce the computational difficulties in modeling a spirally-wound cylindrical Li-ion cell. By analyzing the geometric relations of the winding locus, we confirmed that the charge balance equations can be solved on a 2-D planar surface instead of a 3-D spiral surface without losing much accuracy. We developed a coordinate transform and variable extrusion algorithm; and with these the electrical and thermal variables can be solved and evaluated in the 2-D electrode pair domain and then delivered to the 3-D jelly-roll domain and coupled with the thermal model. The accuracy of variable extrusion could be improved by using more effective approximation approaches to express variables as explicit functions of 2-D coordinates. Our numerical method enables the jelly-roll model to be solved without using extremely fine mesh and thus greatly lowers the memory requirements saves computation time.

Appendix A

Governing equations for the equivalent circuit model (ECM)

The transient response equations of the two R–C branches in the equivalent circuit presented by Fig. 7 are as follow:

$$\frac{\partial Q_p}{\partial t} = -\frac{Q_p}{R_p C_p} + i_{N,(\theta,\theta')} \tag{A1}$$

$$\frac{\partial Q_n}{\partial t} = -\frac{Q_n}{R_n C_n} + i_{N,(\theta,\theta')} \tag{A2}$$

where Q_p and Q_n are respectively the amount of charge (in the unit of C m^{-2}) on the capacitors C_p and C_n. The discharge capacity of the cell stack (in the unit of Ah m^{-2}) is calculated as follow:

$$\frac{\partial Q_{dchg}}{\partial t} = \frac{i_{N,(\theta,\theta')}}{3600\ [\mathrm{s\ h^{-1}}]} \tag{A3}$$

The depth-of-discharge of cell (DOD) is defined as:

$$\mathrm{DOD} = \frac{Q_{dchg}}{Q_0} \tag{A4}$$

where Q_0 is the theoretical maximum cell capacity per unit area of electrode pair. The potential difference over the cell stack is related to the transversal current density through the following expression:

$$\Phi_+(\theta) - \Phi_-(\theta') = U + i_{N,(\theta,\theta')} R_s + \frac{Q_p}{C_p} + \frac{Q_n}{C_n} \tag{A5}$$

Validation of the ECM

In an equivalent circuit model, the electrical components (R_p, C_p, R_n, C_n, R_s, and U) may depend on the depth of discharge (DOD), and these DOD-dependency relationships can be empirically determined by fitting the ECM to real data or results from a full-order physics-based model. In this work, the ECM was validated using the pseudo-2D porous electrode model (P2D model) derived by Doyle et al. [15,16], and the parameters for the P2D model are obtained from reference 7.

The open circuit voltage, U, was fit to a C/100 discharge profile generated by the P2D model (as shown in Fig. A-1) as a cubic spline interpolate function of DOD. The other components were fit to the high power pulse cycle (HPPC) profiles generated by the P2D model at different fixed DOD values. The HPPC simulation protocols include: at a fixed DOD, a 5C discharge current pulse was first applied to the cell for 10 s; rest the cell for 40 s; a 3C charge current pulse was applied for 10 s; rest the cell for 60 s; and then discharge the cell at 1C rate for to next DOD value. The fits of ECM to the P2D-generated HPPC profiles at a specific DOD are presented in Fig. A-2. In this way, the estimated values for electrical components at different DOD values are obtained and the results are listed in Table A-1, and the DOD dependencies of these components on DOD are also approximated using the cubic spline interpolation.

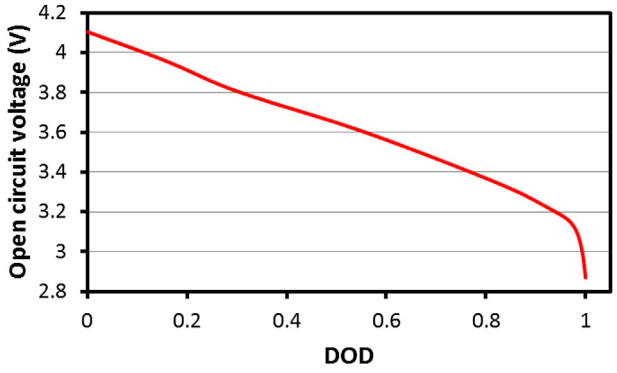

Fig. A-1. Open-circuit voltage profile generated by P2D model.

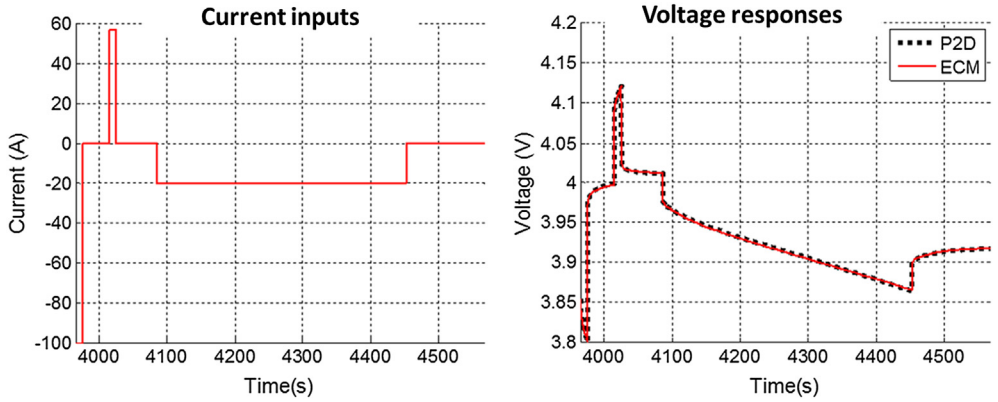

Fig. A-2. Fitting ECM to the HPPC results at a fixed DOD generated by P2D model.

Table A-1
Values for ECM components at different DOD

DOD	R_s [Ω m^2]	R_p [Ω m^2]	C_p [F m^{-2}]	R_n [Ω m^2]	C_n [F m^{-2}]
1.524E-01	2.150E-03	1.058E-03	3.307E+04	2.804E-04	6.242E+03
2.580E-01	2.150E-03	1.127E-03	2.837E+04	2.828E-04	5.383E+03
3.635E-01	2.152E-03	9.919E-04	3.277E+04	2.272E-04	6.678E+03
4.691E-01	2.158E-03	8.594E-04	3.897E+04	2.012E-04	7.738E+03
5.746E-01	2.168E-03	8.202E-04	4.234E+04	2.130E-04	7.386E+03
6.802E-01	2.183E-03	9.186E-04	3.869E+04	2.478E-04	6.230E+03
7.858E-01	2.209E-03	1.022E-03	3.441E+04	2.821E-04	5.405E+03
8.913E-01	2.255E-03	1.034E-03	3.542E+04	3.296E-04	4.680E+03

Appendix B

As discussed in Section 2.9, a variable extruded from the 2-D electrode pair domain to the 3-D jelly-roll domain must be an explicit expression of polar angle θ and coordinate z. Let $\Psi(\xi,z)$ stand for a variable continuously distributed in the 2-D domain$\xi-z$, and $\Psi(\xi,z)$ can be approximated as the following expression:

$$\Psi(\xi,z)\approx\sum_i\sum_j\Psi_{i,j}p_i(\xi)q_j(z) \tag{B1}$$

where $\Psi_{i,j}$ is the value of $\Psi(\xi,z)$ at node point (ξ_i,z_j), and $p_i(\xi)$ and $q_j(z)$ are linear basis functions along the ξ and z directions. The schematic illustration for a linear basis function, $p_i(\xi)$, is presented in Fig. B-1; according to the plot, $p_i(\xi)=1$ at node point $\xi=\xi_i$ and $p_i(\xi)=0$ at all other node points in the ξ direction; and in the two adjacent intervals of node point $\xi=\xi_i$, $[\xi_{i-1},\xi_i]$ and $[\xi_i,\xi_{i+1}]$, $p_i(\xi)$ takes linear profiles. Therefore, $p_i(\xi)$ is a tent function that can be expressed as follow:

$$p_i(\xi)=\frac{\xi_i-\xi_{i-1}+|\xi-\xi_{i-1}|-|\xi-\xi_i|}{2(\xi_i-\xi_{i-1})}-\frac{\xi_{i+1}-\xi_i+|\xi-\xi_i|-|\xi-\xi_{i+1}|}{2(\xi_{i+1}-\xi_i)} \tag{B2}$$

According to Equation (3), ξ is an explicit function of θ, as a result, $\Psi(\xi,z)$ can thus be expressed as an explicit function of θ and z.

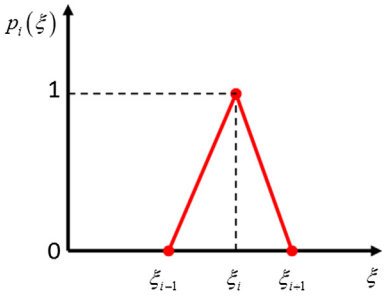

Fig. B-1. Plot for linear basis function.

References

[1] Q. Wang, P. Ping, X. Zhao, G. Chu, J. Sun, C. Chen, J. Power Sources. 208 (15) (2012) 210–224.
[2] R. Spotnitz, J. Franklin, J. Power Sources. 113 (2003) 81–100.
[3] M.C. Smart, B.V. Ratnakumar, J. Electrochem. Soc. 158 (4) (2011) A379–A389.
[4] G.-H. Kim, A. Pesaran, R. Spotnitz, J. Power Sources. 170 (2) (2007) 476–489.
[5] U.-S. Kim, C.-B. Shin, C.-S. Kim, J. Power Sources. 189 (1) (2009) 841–846.
[6] M. Guo, R.E. White, J. Power Sources. 221 (1) (2013) 334–344.
[7] G.-H. Kim, K. Smith, K.-J. Lee, S. Santhanagopalan, A. Pesaran, J. Electrochem. Soc. 158 (8) (2011) A955–A969.
[8] M. Guo, G.-H. Kim, R.E. White, J. Power Sources. 240 (2013) 80–94.
[9] P. Taheri, A. Mansouri, B. Schweitzer, M. Yazdanpour, M. Bahrami, J. Electrochem. Soc. 160 (10) (2013) A1731–A1740.
[10] P.M. Gomadam, R.E. White, J.W. Weidner, J. Electrochem. Soc. 150 (10) (2003) A1339–A1345.
[11] S. Santhanagopalan, P. Ramadass, J. Zhang, J. Power Sources. 194 (2009) 550–557.
[12] Y. Ye, Y. Shi, L.H. Saw, A.O. Tay, J. Power Sources. 243 (2013) 779–789.
[13] K.-J. Lee, K. Smith, A. Pesaran, G.-H. Kim, J. Power Sources. 241 (2013) 20–32.
[14] M. Chen, G.A. Rincon-Mora, IEEE Trans. Energy Convers. 21 (2) (2006) 504–511.
[15] M. Doyle, T. Fuller, J. Newman, J. Electrochem. Soc. 140 (6) (1993) 1526–1533.
[16] S. Santhanagopalan, Q. Guo, P. Ramadass, R.E. White, J. Power Sources. 156 (2) (2006) 620–628.

List of symbols

A_+, A_-: area of the tab-contact surfaces, m^2
C: rate capacity of cell, Ah
C_p, C_n: capacitances in equivalent circuit, F m^{-2}
C_P: specific heat capacity of material, J K^{-1} kg^{-1}
D: separation distance of the Archimedean spiral, m
DOD: depth of discharge
h: heat transfer coefficient in the spaces between cells, W K^{-1} m^{-2}
i_C: transversal current density for C rate, A m^{-2}
$i_{N,(\theta,\theta')}$: transversal current density through a cell stack, A m^{-2}
$i_{v,+}$, $i_{v,-}$: volumetric current source, A m^{-3}
I_{App}: current applied to or from the module, A
$\underline{\underline{\mathbf{k}}}$: matrix for thermal conductivities, W K^{-1} m^{-1}
k_r: thermal conductivity in the normal direction of the spiral surface, W K^{-1} m^{-1}
k_ξ: thermal conductivity in the tangential direction of the spiral surface, W K^{-1} m^{-1}
n_w: index of spiral winding turns
N_w: number of winding turns in a jelly-rolll
N_x, N_y, N_z: heat flux in the x, y, and z directions, W m^{-2}
N_r: heat flux in the normal direction of the spiral surface, W m^{-2}
N_ξ: heat flux in the tangential direction of the spiral surface, W m^{-2}
Q_{dchg}: discharge capacity, Ah m^{-2}
$Q_{EC,(\theta,\theta')}$: volume-average electrochemical heat source through a cell stack, W m^{-3}
$Q_{J,(\theta,\theta')}$: volume-average Joule heat source through a cell stack, W m^{-3}
Q_H: Heat generation rate in the electrode pair domain, W m^{-3}
Q''_H: heat generation rate extruded to the jelly-roll domain, W m^{-3}
Q_p, Q_n: amount of charge on capacitors, C m^{-2}
R_p, R_n: parallel resistances in equivalent circuit, Ω m^2
r: radius coordinate, m
r_0: initial radius for Archimedean spiral, m
t: time, K
T: temperature, s
U: open-circuit voltage, V
x, y, z: Cartesian coordinates, m
α: angle between the normal direction of spiral surface and the x axis, rad
δ_+, δ_-: thickness of current collectors, m
δ_s: thickness of cell stack, m
Φ_+, Φ_-: electric potentials of current collectors, V
θ: polar angle, rad
θ_E: elevation angle, rad
ρ: density of cell, kg m^{-3}
σ_+, σ_-: Electrical conductivity of current collectors, S m^{-1}
ξ: tangential arc length of the spiral surface, m